Commun. Comput. Phys.
doi: 10.4208/cicp.070510.150511s

Vol. **11**, No. 4, pp. 1300-1310
April 2012

Aerodynamic Analysis of a Localized Flexible Airfoil at Low Reynolds Numbers

Wei Kang, Jia-Zhong Zhang* and Pei-Hua Feng

School of Energy and Power Engineering, Xi'an Jiaotong University, Xi'an 710049, Shaanxi, China.

Received 15 May 2010; Accepted (in revised version) 15 May 2011

Available online 30 November 2011

Abstract. A localized flexible airfoil at low Reynolds numbers is modeled and the aerodynamic performance is analyzed numerically. With characteristic based split scheme, a fluid solver for two dimensional incompressible Navier-Stokes equations is developed under the ALE framework, coupled with the theory of shallow arch, which is approximated by Galerkin method. Further, the interactions between the unsteady flow and the shallow arch are studied in detail. In particular, the effect of the self-excited vibration of the structure on aerodynamic performance of the airfoil is investigated deeply at various angles of attack. The results show that the lift-to-drag ratio has been increased greatly compared with the rigid airfoil. Finally, the relationship between the self-excited vibration and the evolution of the flow is analyzed using FFT tools.

AMS subject classifications: 74F10, 76G25, 76D55, 76D05

Key words: Fluid-structure interaction, Navier-Stokes equations, aerodynamic performance, lift enhancement and drag reduction, flow control.

1 Introduction

With the rapid development of the aeronautic technology, the flexible structures (like shell, plate, shallow arch, membrane etc) have been used frequently in the aerospace vehicles, high-performance aircraft and micro air vehicles etc. One advantage of the flexible structures is that it can gain the potential of the shape adaptation for severe flow condition, resulting in delayed separation and what is more, lift enhancement and drag reduction, compared with rigid ones. However, during the flying, the flow and the flexible structures are coupling strongly, giving rise to a rich variety of nonlinear problems

*Corresponding author. *Email addresses:* wkangxjtu@stu.xjtu.edu.cn (W. Kang), jzzhang@mail.xjtu.edu.cn (J.-Z. Zhang), f-peihua@stu.xjtu.edu.cn (P.-H. Feng)

with respect to stability of airfoil, the dynamic response of the flexible structure, unsteady separation, vortex formation and evolution and so on. Therefore, to understand the behaviors of the coupling systems is one of the important issues for the applications of such structures.

Recent studies have begun to focus on the close interaction between the fluid flow and flexible structure for the aeroelastic problems. In 2007, Persson et al. [1] have investigated both fixed and oscillating membrane airfoils using a high-order discontinuous Galerkin method. More recently, Gordnier [2] presented a viscous aeroelastic computation and analysis for a two dimensional flexible membrane airfoil and highlighted the positive impact of the airfoil flexibility. Experimental flow visualizations have been carried out as well. In 2007, Song and Breuer [3] investigated the aerodynamics of the compliant membrane related to mammalian flight by means of wind tunnel tests. In 2009, Rojratsirikul et al. [4] studied unsteady aerodynamics for a two-dimensional membrane airfoil at low Reynolds numbers with a PIV system. The airfoils in these studies have been considered as fully flexible. However, in the practical cases, the fully flexible structures are mainly used in micro air vehicles. For the structure in normal or large size, fully flexible structures would be sensitive to irreversible damages during the flying with high speed. Moreover, it is difficult to implement active control for such kind of airfoils. Thus, the model of the localized flexible airfoil is presented by introducing the theory of shallow arch in this study, which would be a better choice for airfoil design and flow control.

In order to gain a profound understanding of unsteady aerodynamics of the localized flexible structure, an effective algorithm for the problem of fluid-structure interaction should be established and developed first in such situation. Many approaches have been suggested for this kind of problems (see [5–9]). One of the methods used commonly is the Arbitrary Lagrangian Eulerian method (ALE) [5, 6]. In this study, characteristics based split (CBS) scheme is chosen for fluid-structure interaction under the ALE framework. The CBS scheme was first introduced into the governing equations of fluid by Zienkiewicz in 1995. Its basic idea is the approximation of the characteristics by using a Taylor expansion with a split procedure and it has been successfully used in computational fluid dynamics and computational structural dynamics [10–13]. However, this algorithm is not suitable for the fluid-structure interaction problems and needs to be extended. Hence, a CBS algorithm under the ALE framework is developed to deal with the problems relevant to fluid-structure interaction and an implicit approximation for CBS scheme is implemented consequently in this study.

The purpose of the study is the computational aeroelasticity of the localized flexible airfoil at low Reynolds numbers. The impacts of coupling between the fluid and the structure on the aerodynamic performance are investigated in comparison with the rigid airfoil. The results also show the relationship between the flow evolution and dynamic motion of the flexible structure.

2 Aerodynamic solver

2.1 Navier-Stokes equations under the ALE framework

When the Mach number is less than 0.3, the flow is considered as incompressible. Let L be the characteristic scale, u_L be the characteristic velocity and dimensionless variables are defined as

$$x^*=\frac{x}{L}, \qquad y^*=\frac{y}{L}, \qquad t^*=\frac{u_L t}{L},$$
$$p^*=\frac{p}{\rho u_L^2}, \qquad u^*=\frac{u}{u_L}, \qquad v^*=\frac{v}{u_L}.$$

For the sake of simplicity, the $(*)$ is dropped here and the governing equation for two-dimensional unsteady incompressible flow in the ALE configuration can be written as

$$\frac{\partial u_i}{\partial x_i}=0,$$
$$\frac{\partial u_i}{\partial t}+(u_j-\widehat{u}_j)\frac{\partial u_i}{\partial x_j}=-\frac{\partial p}{\partial x_i}+\frac{1}{Re}\frac{\partial^2 u_i}{\partial x_j \partial x_j},$$
$$Re=\frac{\rho u_L L}{\mu},$$

where $\widehat{u}_j$ the velocity of the grid ρ and u_i is the density and velocity of the fluid, respectively.

The boundary conditions in this problem are listed as follows:

- The boundary on which the velocity needs to be specified is denoted by $(\Gamma_t)_g \subset \Gamma_t = \partial\Gamma_t$,

$$u_i=(u_i)_g \quad \text{on} \quad (\Gamma_t)_g \subset \Gamma_t=\partial\Omega_t. \tag{2.1}$$

- The boundary on which the tractions are prescribed is denoted by $(\Gamma_t)_h \subset \Gamma_t$,

$$n_j\cdot\sigma_{ij}=(\sigma_i)_h \quad \text{on} \quad (\Gamma_t)_h \subset \Gamma_t=\partial\Omega_t. \tag{2.2}$$

2.2 ALE-CBS scheme

When solving Navier-Stokes equation using standard finite element method, if Reynolds number is too higher, the numerical solution will oscillate and become unstable because of nonlinear convective terms. In order to solve this problem, new coordinates along the characteristic line are introduced. After the coordinate transformation, convective terms are removed and the resulting equations are the simple diffusion equations, which can be solved by the standard finite element method.

There are three steps for solving the resulting equations by introducing an operator split procedure in temporal discretization before spatial discretization. The CBS procedures are summed up as below and the detailed derivation of CBS scheme can be referred to [14].

Step 1 Obtain intermediate velocities.

$$U_i^*-U_i^n=\Delta t\Big(-c_j\frac{\partial}{\partial x_j}(U_i^n)+\frac{1}{Re}\frac{\partial^2 U_i^n}{\partial x_j\partial x_j}\Big)+\frac{\Delta t^2}{2}c_k\frac{\partial}{\partial x_k}\Big(\frac{\partial}{\partial x_j}(c_jU_i^n)+\frac{1}{Re}\frac{\partial^2 U_i^n}{\partial x_j\partial x_j}\Big), \tag{2.3}$$

where $c_j=u_j-\widehat{u}_j$.

Step 2 Solve the continuity equation implicitly.

$$\theta_1\Big(\frac{\partial^2 p^n}{\partial x_i\partial x_i}\Big)=\frac{1}{\Delta t}\Big(\theta_1\frac{\partial U_i^*}{\partial x_i}+(1-\theta_1)\frac{\partial U_i^n}{\partial x_i}\Big). \tag{2.4}$$

Step 3 Correct the velocities with obtained pressure.

$$U_i^{n+1}-U_i^*=-\Delta t\frac{\partial p^n}{\partial x_i}. \tag{2.5}$$

Eqs. (2.3), (2.4) and (2.5) are the temporal discretization form of Navier-Stokes equations with CBS scheme and these equations can be approached by the standard finite element method. The domain of flow field is meshed by unstructured triangular element. And then linear shape functions in the same order are used for the velocities and pressure in the spatial discretizing.

3 Model of a localized flexible airfoil and its approaching

3.1 Structure model

For the structure part of the simulation, shallow arch is used for the localized flexible airfoil model. A part of the airfoil surface is an elastic shallow arch with simply supported boundary. Fig. 1 shows the shallow arch with simply supported boundaries, subjected to normal aerodynamic pressure.

The analysis for the shallow arch will be carried out under the following assumptions: (1) the deformation is elastic; (2) the shearing deformation and rotary inertia are ignored; (3) the geometric nonlinearity is considered; (4) the damping is introduced.

Following the Hamilton's principle and using the chord of the airfoil and the freestream density and velocity of the flow as characteristic length and velocity, the governing equation in dimensionless form for the shallow arch can be presented as follows,

$$\rho h\frac{\partial^2 w}{\partial t^2}+\frac{Eh^3}{12}w''''+V(y_0''-w'')+d\frac{\partial w}{\partial t}=\Delta p, \tag{3.1}$$

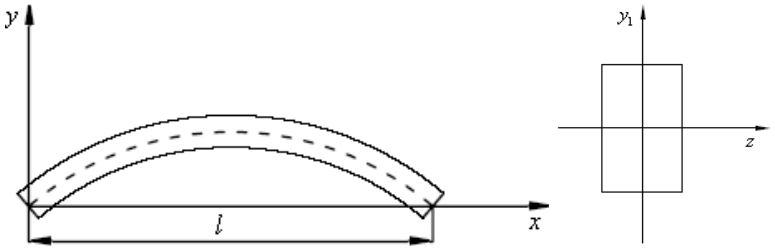

Figure 1: Schematics of shallow arch.

where h is the thickness of the arch, d is the dimensionless damping per area, ρ the density ratio of the arch to the fluid, $V=l^{-1}\int_0^l[\frac{Eh}{2}(y'^2-y_0'^2)]dx$ and the dimensionless pressure force Δp is obtained from the aerodynamic solver.

Finally, the simple supported boundary conditions are described as

$$w|_{x=0}=w|_{x=l}=0 \tag{3.2}$$

and the initial position and the initial velocity of the shallow arch in the flow can be described as

$$t=0:\quad w=0,\quad \frac{\partial w}{\partial t}=0. \tag{3.3}$$

The initial shape or configuration of the shallow arch is assumed as follows,

$$\begin{cases} y_0(x)=\sum_{i=1}^{5}a_i x^i, \\ x=0,\quad y_0(0)=0, \\ x=l,\quad y_0(l)=0. \end{cases} \tag{3.4}$$

3.2 Numerical method for the structure model

In order to obtain the numerical solution of the structure modal, Galerkin method is used in this Section [15].

The linear operator of Eq. (3.1) together with the boundary conditions Eq. (3.2) can be defined as $Lw=Eh^3w''''/12$. Then $\{\sin(n\pi/l)x,\ n=1,2,\cdots,+\infty\}$ constitute the complete set of eigenfunctions of the operator, which span an orthogonal basis of the space which the solution of the governing equation will be projected onto. The Galerkin procedure is used to approach the solution, that is

$$w(x,t)=\sum_{n=1}^{\infty}w_n(t)\sin\frac{n\pi}{l}x. \tag{3.5}$$

Let

$$G(x,y,w)=\frac{Eh^3}{12}w''''+V(y_0''-w'')+\rho h\frac{\partial^2 w}{\partial t^2}+d\frac{\partial w}{\partial t}-\Delta p. \tag{3.6}$$

Following Galerkin procedure, yields

$$\int_0^l G(x,y,w)\sin\frac{m\pi}{l}x=0, \qquad m=1,2,3,\cdots,+\infty. \tag{3.7}$$

The general form of Eq. (3.7) can be obtained as

$$\begin{aligned}&\frac{Eh^3}{12}w_m\frac{(m\pi)^4}{2l^3}+\sum_{n=1}^{\infty}\left\{w_n^2\frac{(n\pi)^2}{2l}\frac{Eh}{2l}+\frac{2Ebh}{n\pi}w_n[(-1)^{n+1}+1]\right\}2b\frac{l}{m\pi}[(-1)^{m+1}+1]\\&+\sum_{n=1}^{\infty}\left\{w_n^2\frac{(n\pi)^2}{2l}\frac{Eh}{2l}+\frac{2Ebh}{n\pi}w_n[(-1)^{n+1}+1]\right\}w_m\frac{(m\pi)^2}{2l}\\&+\frac{\rho hl}{2}\ddot{w}+\frac{ld}{2}\dot{w}-\int_0^l\Delta p\sin\frac{m\pi}{l}xdx=0, \qquad m=1,2,\cdots,+\infty.\end{aligned} \tag{3.8}$$

Eq. (3.8) can be solved by coupling with the aerodynamic solver and then the dynamic behaviors of the localized flexible airfoil can be obtained.

4 Mesh moving technique

When dealing with fluid-structure interaction, the mesh must conform to the instantaneous deformation of the structure. In this study, the spring analogy based on Blom's algorithm [16] is adopted for the mesh moving. The moving mesh in each time step is considered as a balance spring system with a network of fictitious springs. The elastic coefficients of the springs are related to the edge of the elements and torsion effect related to the angles of the elements. The new position of dynamic mesh is determined by the equilibrium condition requiring that the sum of spring forces at each internal node be zero. The mesh moving technique has proven efficient for the aerodynamic and structural coupling. The scheme needs less than 3000 times iterations per time step before it satisfies the given precision.

5 Results and discussions

5.1 Verification

In order to verify the algorithm, the laminar flow induced by the harmonic in-line oscillation of a circular cylinder in water at rest is simulated numerically. Define the maximum velocity of the oscillating circular cylinder as characteristic velocity, the diameter of the circular cylinder as characteristic length. Hence the key numbers, Reynolds number Re and the Keulegan-Carpenter number KC are defined as

$$Re=\frac{\rho U_m d}{\mu}, \qquad KC=\frac{U_m}{fd}, \tag{5.1}$$

where f denotes the oscillating frequency of the cylinder.

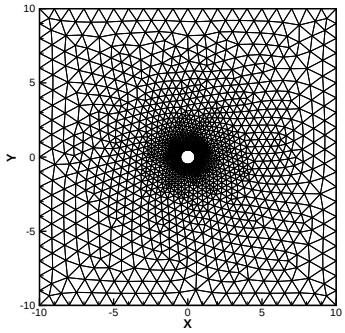

Figure 2: Schematics of computational grid.

The translational motion of the cylinder is given by the harmonic oscillation,

$$x_c(t) = -A_m \sin(2\pi f t), \tag{5.2}$$

where A_m stands for the amplitude of the oscillating cylinder and thus the Keulegan-Carpenter number can be rewritten as $KC = 2\pi A_m / d$.

In this numerical example, the key parameters are set as $Re = 100$ and $KC = 5$. The computational domain is $-8d \leqslant x \leqslant 8d$, $-6d \leqslant y \leqslant 6d$, where d is the diameter of the cylinder, meshed by unstructured triangular grids (see Fig. 2). The computation is performed by the presented algorithm, compared with the existed experiment [17]. The results shows a good agreement between the presented algorithm and the experiment from [17], shown in Fig. 3. It can prove that the algorithm is feasible for fluid-structure interaction.

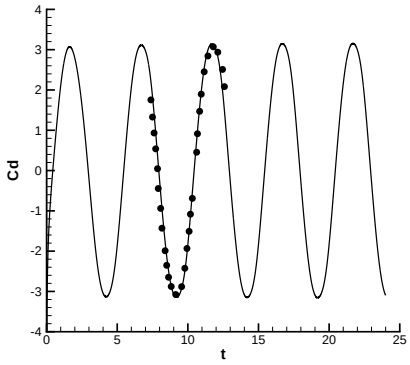

Figure 3: Comparison of drag coefficients between the presented algorithm (–) and [17] (•).

5.2 Aerodynamic analysis of the localized flexible airfoil

In the section, the aerodynamic performance of NACA 0015 airfoil with localized flexibility is studied. The part of the airfoil surface from the leading edge to the one third chord is an elastic surface. The dimensionless structural parameters of the shallow arch are listed in Table 1.

Table 1: Dimensionless structural parameters of the shallow arch.

mode	thickness	damping	elastic modulus	density
7	0.001	0.5	1.2×10^6	7850

Table 2: The relative rate of the lift and drag coefficients between the flexible and rigid airfoil (positive-increase; negative-decrease).

Angles of attack	relative rate of Cl %	relative rate of Cd %	relative rate of Cl/Cd %
4	0.9	10	-8.26899
8	3.16	-0.51	3.68909
10	5.7138	-7.26	13.98204
11	12.68	-2.56	15.64645
12	7.72	-20.38	35.29186
13	3.7048	-37.02	64.65907
14	6.94	-43.27	88.51138
15	18.69	-35.52	84.07863
16	23.48	-33.45	85.53006

Fig. 4 shows the comparison of the lift and drag coefficients between the flexible airfoil and rigid one at angles of attack $\alpha=4\sim16^\circ$ and $Re=2\times10^5$. The results indicate that the self-excited vibration of the flexible airfoil can improve the aerodynamic performance greatly, compared with the rigid airfoil. The stall angle has been delayed from about 13° to about 16°. At $\alpha=11^\circ$, the lift coefficients increase 12.68%, due to the oscillation. When the angle of attack reaches $\alpha=16^\circ$, the lift coefficient increases up to 23.48% compared with that of rigid airfoil. The drag is also reduced. In Table 2, the drag coefficients gains more than 30% reduction when the angles of attack are higher than 13°. Furthermore, the results show that due to the self-excited vibration of the flexible airfoil, the lift-drag ratio is increased greater than 80% at higher angles of attack.

In order to reveal the detail of the interactions between the flexible airfoil and un-

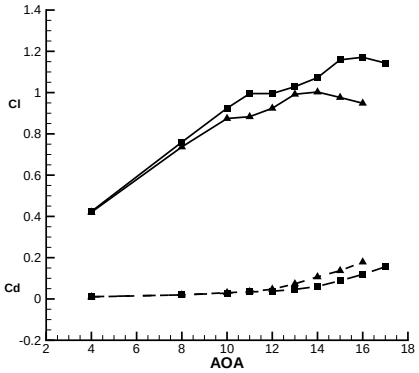

Figure 4: The comparison for lift and drag coefficients between the localized flexible (■) and rigid airfoil (▲).

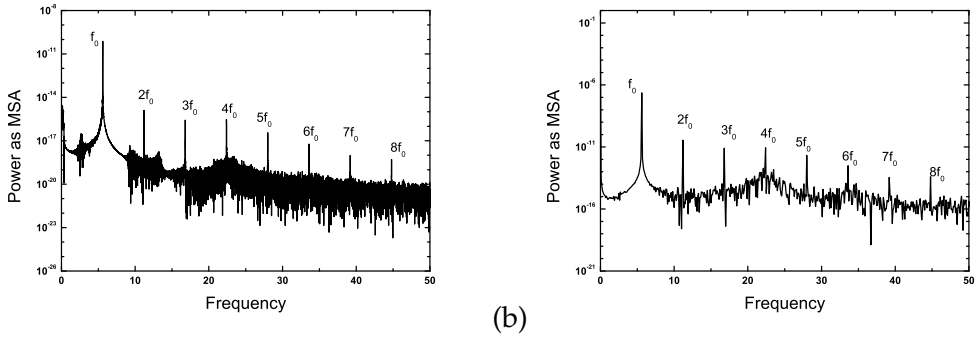

Figure 5: Power spectrums of the middle point on the flexible surface (a) and pressure at point $(1,-0.4)$ in the flow (b) at (MSA means mean squared amplitude) at $\alpha=8^\circ$.

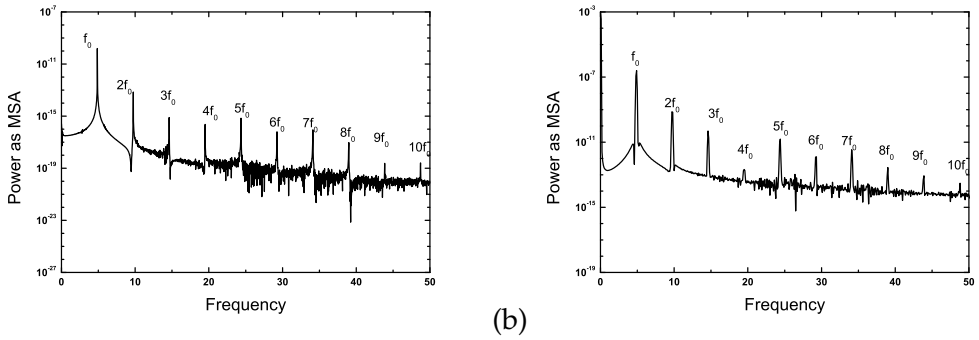

Figure 6: Power spectrums of the middle point on the flexible surface (a) and pressure at point $(1,-0.4)$ in the flow (b) at $\alpha=11^\circ$.

steady flow, spectrum analysis, for both the pressure fluctuation at the given point in the flow and velocity fluctuation at middle point of the shallow arch are carried out (see Figs. 5, 6). The point in the flow is chosen near the trailing edge of the airfoil, where the shedding vortices are passing. It is also far away from the self-excited vibrating part of the airfoil. At low angle of attack $\alpha=8^\circ$, in Fig. 5(a), there exists a series of peaks at the primary frequency $f_0=5.59944$ and its harmonic frequencies $2f_0,\cdots,8f_0$ for the flow, while the dynamic response for the shallow arch presents the same frequency band. The frequencies of two dynamic systems, the shallow arch system and the flow, are closed to each other during the interaction, which is the synchronization phenomenon. When the angle of attack increases to 11°, power spectrum for the flow and the shallow arch contain ten peaks at the primary frequency $f_0=4.8995$ and its harmonic frequencies $2f_0,\cdots,10f_0$. This can be implied that the synchronization phenomenon exists in the coupling between the structure and the fluid at low angles of attack. At higher angle of attack $\alpha=16^\circ$, the response of the structure becomes less regular (see Fig. 7). Multiple frequency bands are observed both in the structural response and computed vortex shedding. However, the synchronization phenomenon no longer occurs. The frequencies between the structure response and vortex shedding do not match each other.

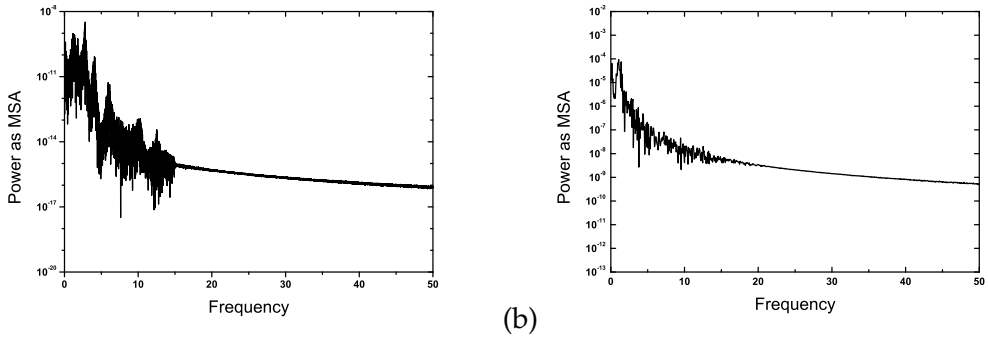

(a) (b)

Figure 7: Power spectrums of the middle point on the flexible surface (a) and pressure at point $(1,-0.4)$ in the flow(b) at $\alpha=16^\circ$.

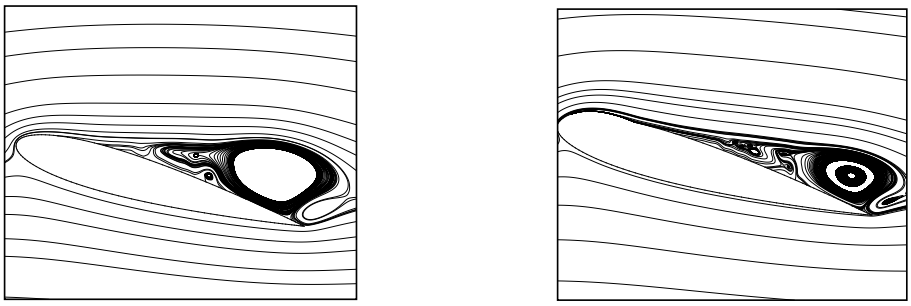

(a) the rigid airfoil (b) the localized flexible airfoil

Figure 8: Streamline near the airfoil at $\alpha=16^\circ$.

Mean flow field for the rigid airfoil and the localized flexible airfoil at $\alpha=16^\circ$ are presented to demonstrate the effect of self-excited vibration of the flexible airfoil on the streamline topology in Fig. 8. For the rigid airfoil, there exists a dominant vortex above the upper surface of the airfoil in the flow field. However, the dominant vortex is reduced significantly due to more vortices in small sizes dissipating the energy of the dominant vortex. Furthermore, the thickness of shear layer is also reduced due to the self-adaption of the flexible airfoil.

6 Conclusions

From the above analysis, the results show that the ALE-CBS algorithm presented is feasible for the fluid-structure interaction of flexible airfoil involving both structure and fluid nonlinearities. The self-excited vibration of the localized flexible airfoil can improve the aerodynamic performance significantly. The lift-drag ratio is greater than 80% at higher angles of attack and the stall angle is also delayed from about 13° to 16°. For two coupling dynamic systems, namely the shallow arch system and the flow, the synchronization phenomenon is captured by FFT analysis at low angles of attack. The self-adaption

of the flexible airfoil can reduce the size of the dominant vortex and the thickness of shear layer.

Acknowledgments

This research is supported by Program for New Century Excellent Talents in University in China, No. NCET-07-0685.

References

[1] P. Persson, J. Peraire and J. Bonet, A high order discontinuous galerkin method for fluid-structure interaction, AIAA Computational Fluid Dynamics Conference, Citeseer, 25–28.
[2] R. Gordnier, High fidelity computational simulation of a membrane wing airfoil, J. Fluids Struct., 25 (2009), 897–917.
[3] A. Song and K. Breuer, Dynamics of a compliant membrane as related to mammalian flight, AIAA paper, 2007-665.
[4] P. Rojratsirikul, Z. Wang and I. Gursul, Unsteady fluid-structure interactions of membrane airfoils at low reynolds numbers, Animal Locomotion, 1 (2010), 297.
[5] P. Kjellgren and J. Hyvärinen, An arbitrary lagrangian-eulerian finite element method, Comput. Mech., 21 (1998), 81–90.
[6] J. Sarrate, A. Huerta and J. Donea, Arbitrary lagrangian-eulerian formulation for fluid-rigid body interaction, Comput. Methods Appl. Mech. Eng., 190 (2001), 3171–3188.
[7] D. Kim and H. Choi, Immersed boundary method for flow around an arbitrarily moving body, J. Comput. Phys., 212 (2006), 662–680.
[8] R. Li, T. Tang and P. Zhang, Moving mesh methods in multiple dimensions based on harmonic maps, J. Comput. Phys., 170 (2001), 562–588.
[9] Y. Di, R. Li, T. Tang and P. Zhang, Moving mesh finite element methods for the incompressible Navier-Stokes equations, SIAM J. Sci. Comput., 26 (2005), 1036–1056.
[10] B. Celik and F. Edis, Analysis of fluid flow through micro-fluidic devices using characteristic-based-split procedure, Int. J. Numer. Methods Fluids, 51 (2006), 1041–1057.
[11] J. Rojek, E. Oñate and R. Taylor, CBS-based stabilization in explicit solid dynamics, Int. J. Numer. Methods Eng., 66 (2006), 1547–1568.
[12] P. Nithiarasu, A fully explicit characteristic based split (CBS) scheme for viscoelastic flow calculations, Int. J. Numer. Methods Eng., 60 (2004), 949–978.
[13] P. Nithiarasu, R. Codina and O. Zienkiewicz, The characteristic-based split (CBS) scheme, a unified approach to fluid dynamics, Int. J. Numer. Methods Eng., 66 (2006), 1514–1546.
[14] O. Zienkiewicz and R. Codina, A general algorithm for compressible and incompressible flowłpart I: the split, characteristic-based scheme, Int. J. Numer. Methods Fluids, 20 (1995), 869–885.
[15] J. Zhang, Y. Liu, P. Lei and X. Sun, Dynamic snap-through buckling analysis of shallow arches under impact load based on approximate inertial manifolds, Dynam. Cont. Dis. Ser. B, (DCDIS-B), 14 (2007), 287–291.
[16] F. Blom, Considerations on the spring analogy, Int. J. Numer. Methods Fluids, 32 (2000), 647–668.
[17] H. Dütsch, F. Durst, S. Becker and H. Lienhart, Low-reynolds-number flow around an oscillating circular cylinder at low keulegan–carpenter numbers, J. Fluid Mech., 360 (1998), 249–271.